### Title

Intraoperative application and early experience with novel high-resolution, high-channel-count thin-film electrodes for human microelectrocorticography.




### Journal

Journal of Neurosurgery, 140(3)



### Authors

Tan, Hao

Paulk, Angelique

Stedelin, Brittany

et al.



### Publication Date

2024-03-01

### DOI

10.3171/2023.7.JNS23885

Peer reviewed

HHS Public Access

Author manuscript

*J Neurosurg*. Author manuscript; available in PMC 2024 May 20.

Published in final edited form as:

*J Neurosurg*. 2024 March 01; 140(3): 665–676. doi:10.3171/2023.7.JNS23885.

# Intraoperative application and early experience with novel high-resolution, high-channel-count thin-film electrodes for human microelectrocorticography

**Hao Tan, BS**[1], **Angelique C. Paulk, PhD**[2,3], **Brittany Stedelin, BS**[1], **Daniel R. Cleary, MD, PhD**[1,4], **Caleb Nerison, BS**[1], **Youngbin Tchoe, PhD**[5,6,10], **Erik Brown, MD, PhD**[1,7], **Andrew Bourhis, MS**[5], **Samantha Russman, MS**[5], **Jihwan Lee, MS**[5], **Karen Tonsfeldt, PhD**[5,8], **Jimmy C. Yang, MD**[2,3], **Hongseok Oh, PhD**[5,9], **Yun Goo Ro, PhD**[5,9], **Keundong Lee, PhD**[5], **Mehran Ganji, PhD**[5], **Ian Galton, PhD**[5], **Dominic Siler, MD, PhD**[1], **Seunggu Jude Han, MD**[12], **Kelly L. Collins, MD**[1,11], **Sharona Ben-Haim, MD**[4], **Eric Halgren, PhD**[13], **Sydney S. Cash, MD, PhD**[2,3], **Shadi Dayeh, PhD**[5], **Ahmed M. Raslan, MD**[1]

[1]Department of Neurological Surgery, Oregon Health & Science University, Portland, Oregon;

[2]Department of Neurology, Massachusetts General Hospital, Boston, Massachusetts;

[3]Harvard Medical School, Boston, Massachusetts;

[4]Department of Neurological Surgery, University of California San Diego, San Diego, California;

[5]Department of Electrical and Computer Engineering, University of California San Diego, San Diego, California;

[6]Department of Biomedical Engineering, Ulsan National Institute of Science and Technology, Ulsan, Korea;

[7]Department of Neurological Surgery, Nicklaus Children's Hospital, Miami, Florida;

[8]Department of Obstetrics, Gynecology, and Reproductive Sciences, Center for Reproductive Science and Medicine, University of California San Diego, La Jolla, California;

[9]Soongsil University, Seoul, Korea;

[10]Ulsan National Institute of Science and Technology, Ulsan, Korea;

[11]Papé Family Pediatric Research Institute, Oregon Health & Science University, Portland, Oregon;

[12]Department of Neurological Surgery, Stanford University, Palo Alto, California

[13]Department of Neurology, University of California San Diego, San Diego, California;

## Abstract

**OBJECTIVE—**The study objective was to evaluate intraoperative experience with newly developed high-spatial-resolution microelectrode grids composed of poly(3,4-

Corresponding Author Ahmed M. Raslan: Department of Neurological Surgery, Oregon Health & Science University, Mail Code CH8N, 3303 South Bond Avenue, Portland, OR 97239, Fax: 503 346 6810, raslana@ohsu.edu.

ethylenedioxythiophene) with polystyrene sulfonate (PEDOT:PSS), and platinum nanorods (PtNRGrids).

**METHODS—**A cohort of patients who underwent craniotomy for pathological tissue resection and who had high-spatial-resolution microelectrode grids placed intraoperatively were evaluated. Patient demographic and baseline clinical variables, and relevant microelectrode grid characteristic data were collected. The primary and secondary outcome measures of interest were successful microelectrode grid utilization with usable resting state or task-related data, and grid-related adverse intraoperative events and/or grid dysfunction.

**RESULTS—**Included in the analysis were 89 cases of patients who underwent a craniotomy for resection of neoplasms (n = 58) or epileptogenic tissue (n = 31). These cases accounted for 94 grids; 58 PEDOT:PSS grids and 36 PtNRGrids. Of these 94 grids, 86 were functional and used successfully to obtain cortical recordings from 82 patients. Mean cortical grid recording duration was 15.3 ± 1.15 minutes. Most recordings from patients were obtained during experimental tasks (n = 52, 58.4%), involving language and sensorimotor testing paradigms, or obtained passively during resting state (n = 32, 38.1%). There were no intraoperative adverse events related to grid placement. However, there were instances of PtNRGrid dysfunction (n = 8) related to damage incurred by suboptimal preoperative sterilization (n = 7) and improper handling (n = 1); intraoperative recordings were not performed. Vaporized peroxide (V-PRO) sterilization was the most optimal sterilization method for PtNRGrids, providing a significantly greater number of usable channels post-sterilization than steam-based sterilization techniques (905.0 [650.8–935.5] vs. 356.0 [18.0 – 597.8], p = 0.0031).

**CONCLUSIONS—**High-spatial-resolution microelectrode grids can be readily incorporated into appropriately selected craniotomy cases for clinical and research purposes. Grids are reliable when preoperative handling and sterilization considerations are accounted for. Future investigations should compare the diagnostic utility of these high-resolution grids to commercially available counterparts and assess whether diagnostic discrepancies relate to clinical outcomes.

### Keywords

Mapping; Intraoperative; Electrocorticography; Gamma-Band; Passive; High-Resolution; Cortical

## Introduction

Intraoperative functional cortical localization is critical for achieving successful outcomes after brain surgery. Several methods are used to achieve such outcomes including preoperative functional imaging studies and intraoperative neurophysiologic testing through techniques such as somatosensory evoked potential (SSEP) phase reversal for central sulcus localization, direct electrical cortical stimulation mapping, and subcortical stimulation.[1,2] More recently, intraoperative passive high gamma (70–170Hz) mapping (HGM) has emerged as a viable method for localizing functional cortical regions without electrical stimulation.[3,4] This has been shown to help potentially better inform intraoperative surgical decision making.[5,6]

Passive HGM relies on electrocorticography (ECoG) through subdural strips or grids. Current commercially available US Food and Drug Administration (FDA)-approved clinical

ECoG grids have spatial resolution constraints in the form of 10 mm pitch on average with an electrode density of 1 electrode/cm$^2$, although higher density clinical grids can be condensed below an interelectrode distance (pitch) of 4mm to improve resolution. [7] Furthermore, these grids are situated on a plastic mold that has difficulty conforming to the cortical surface without manual handling, which in our experience, can cause discomfort to patients during awake procedures (*investigator(s) personal observations*).

In light of these limitations, a four-institution research collaboration between Oregon Health & Science University, University of California San Diego, Massachusetts General Hospital, and Brigham Women's Hospital has developed ECoG grids composed of thin-film poly(3,4-ethylenedioxythiophene) with polystyrene sulfonate (PEDOT:PSS) and platinum nanorod grids (PtNRGrids).[8,9] These material compositions circumvent the limitations of existing clinical ECoG designs and allow for higher spatial resolution (44–100/cm$^2$), and improved delineation of cortical regions of functional importance.[10–12]

Here we describe our collected experience using high-spatial-resolution PEDOT:PSS and PtNRGrids for cortical surface recording. The primary and secondary outcome measures in patients who underwent a craniotomy procedure were successful microelectrode grid utilization with usable resting state or task-related data, and grid-related adverse intraoperative events and/or grid dysfunction. An overview of procedural considerations related to grid use, for neurosurgeons, is also provided.

## Methods

### Study Design and Patient Selection

Patient data were obtained from all adult patients who consented to the placement of high-resolution microelectrode grids during a craniotomy for resection of pathological tissue. Data was collected from January 1$^{st}$, 2019 to September 10$^{th}$, 2021 for both PEDOT:PSS and PtNRGrids, and through April 1$^{st}$ 2022 for PEDOT:PSS grids, at Oregon Health & Science University, University of California San Diego, Brigham Women's Hospital, and Massachusetts General Hospital. This study was approved by the institutional review boards at all participating institutions (SMART IRB: 4838); subject consent was obtained. Strengthening the Reporting of Observational Studies in Epidemiology (STROBE) reporting guidelines were followed.[13]

### Demographic, Clinical, and Intraoperative Variables

Demographic variables of interest included age and sex. Clinical variables of interest included indication for surgery, institution where surgery and grid placement were performed, and preoperative functional deficits. Intraoperative variables of interest included type of anesthesia used and clinical mapping modalities employed.

### Microelectrode Grid Characteristics of Interest and Outcomes Measures

Microelectrode grid data included chemical composition, number of channels, microelectrode placement strategy, and intracranial location of microelectrode placement. Electrophysiology data collected during recordings are as previously reported.[10–12,14]

Successful use of grids for cortical recording, presence of intraoperative complications and adverse events related to grid use, and instances of microelectrode dysfunction and failure served as primary and secondary outcomes of interest. Additionally, adverse event data included instances of intraoperative cortical tissue damage following grid use, evidence of tissue damage on immediate postoperative imaging studies, and infection within 90-days after surgery.

## PEDOT:PSS and PtNRGrid Chemical Composition and Configuration

Electrode grids were PEDOT:PSS and PtNRGrids (Figure 1). Specifications and nuanced differences between grid specific material compositions are as previously published.[10] In summary, PEDOT:PSS are composed of thin-film poly(3,4-ethylenedioxythiophene) with polystyrene sulfonate. PtNRGrids are composed of elemental platinum, the most widely used biocompatible electrode material, and offer greater stability *in vivo*.[9,15] Grids measuring 32mm x 32mm in size were composed of 1024 channels. Grids measuring 48mm x 48mm in size with 2048 channels were used in two cases. 128 channel grids had three conformations; 1) two 64-channel columns with 50μm pitch, 2) two 64-channel columns with 800μm pitch, and 3) a 4mm diameter circular grid.[12]

## Microelectrode Grid Handling

All microelectrode grids were custom manufactured at the University of California San Diego Integrated Electronics and Biointerfaces Laboratory (IEBL) and received within 2 weeks of an order request. Given microelectrode grid malleability and delicate nature, electrodes were packaged securely in DuraHolder Instrument Protection System (Key Surgical) pouches to minimize mechanical damage during the shipping process (Figure 2A). Once received, grids were typically stored within the packaging material, in a temperate environment with low to moderate humidity (between 50–75°F), until use.

Microelectrode grids were maintained on a flat surface to prevent damage before and during transportation for sterilization or to the operating room (OR). If a microelectrode grid was handled, staff were advised and trained to hold vertically by the bonded extension board so that the microelectrode grid was suspended downward. As such, unwanted contact between any given electrode and immediate surroundings were minimized (Figure 2B).

## Microelectrode Grid Sterilization

Microelectrode grid sterilization techniques have been described previously.[10,16] Following the method of Uguz et al. 2016,[16] PEDOT:PSS grids; were steam sterilized with a steam-based gravity cycle in the autoclave of 250°F/121°C for 30 minutes followed by at least 20 minutes of dry time. For PtNRGrids, a 28-minute non-lumen vaporized peroxide (V-PRO) cycle, which involves aerosolization of hydrogen peroxide was used. PtNRGrids in their DuraHolder pouches were placed on a 470mm x 274mm x 90mm anodized tray with perforated bottoms enclosed within a SterilContainerTM system (Aesculap Surgical Technologies), allowing two grids to be sterilized simultaneously per cycle (Figure 2A). Electrode grids were typically used within 6 days of sterilization.

## Operating Room Preparation

Sterilized grids were transferred to a Mayo Stand and the extension board inserted through a ~10cm opening within the Situate Sterile Drape (Figure 2B). Another smaller opening was created to pass touch-proof connectors for a pair of sterile subdermal needle electrodes, which serve as separate reference and ground electrodes placed in the temporalis muscle or scalp. Then, Tegaderm was used to securely seal the drape openings (Figure 2B). While sterile staff engaged in sterile technique to secure the sterile component of the extension board in place, another non-sterile member of the team on the other side of the drape connects the extension board to an amplifier board (Figure 2C). The drape is then pulled by a nonsterile member of the team over the amplifier board and its outgoing serial peripheral interface (SPI) cables (Figure 2D). Channel yield and impedance testing is then performed prior to placement (Figure 2E). Once the electrode is satisfactorily positioned over cortical regions of interest, Greenberg or C clamps were fastened to the acquisition board to secure the grid in place (Figure 2F). At this point, the recording set-up is complete and ready for signal acquisition (Figure 2G). An overview of teams' workflow process is shown in supplementary figure A.

## Electrophysiologic Data Collection and Signal Processing

All microelectrode grid were placed after clinical passive HGM but before standard electrical stimulation mapping. Final grid placement was documented in 3-dimensional space using a Stealth neuronavigation system and/or surgical microscope snapshots. Post-use channel yield and impedance data was collected in the OR after recordings were completed. Following use, microelectrode grids were re-sterilized and placed in storage.

Electrophysiologic data was collected using an Intan (Intan Technologies LLC, LA, CA) 1024-channel recording system sampled at 20 or 30 kHz with a voltage scale of −5mV to 5mV at a time scale of 200ms or an ORH128 Intan Recording System. ORH128 Intan Recording System data is acquired at 30 kHz and filtered by the default Intan setting, with cutoffs 1 Hz to 7.5 kHz using the OpenEphys acquisition graphic-user interface software (http://www.open-ephys.org/).[17] Electrode impedance testing during the experiments involved Intan RHD2000 software from Intan Technologies (Los Angeles, CA). The Intan amplifier was set to a sampling rate of 20kHz with a bandwidth of 7.6kHz. Electrodes with more than 1000 channels were recorded with customized amplifier boards and Intan recording controllers were used to stream recorded data, which were spatially mapped with a recording laptop using in house MATLAB scripts (Mathworks, Inc. Natick, MA). Channels with impedance magnitudes above 100 kΩ *in vivo* at 1 kHz were excluded from analysis. Neighboring channels with diminished impedance magnitude were evaluated for potential shorts. All recorded signals underwent removal of 60 Hz line noise and harmonics with digital notch filters. Offline analyses were conducted using custom, in-house scripts in MATLAB.

## Statistical Analysis

Statistics were largely descriptive in nature and performed using GraphPad Prism V9.0 with a significance threshold of $\alpha = 0.05$. Categorical and dichotomous variables were reported

as counts and percentages. Continuous variables were reported as mean ± standard error or median [interquartile range] and compared using nonparametric Mann Whitney U-tests.

## Results

### Patient Demographics

Between January 1st, 2019 to April 1st, 2022, 89 patients had 94 grids placed during a craniotomy procedure for resection of pathological tissue. Mean patient age was 45.9 ± 1.7 years with 63.0% and 24.7% operated on at OHSU and MGH, respectively (Table 1). Resection of intracranial neoplasms was the most frequent indication for surgery (65.2%). Most patients had no deficits preoperatively and underwent an awake craniotomy with monitored anesthesia care (68.5%) (Table 1).

### Microelectrode Grids

Between January 1st, 2019 and September 10th, 2021 36 PtNRGrids were placed. Between January 1st, 2019 and April 1st 2022 58 PEDOT:PSS grids were placed. Overall, 32mm x 32mm 1024-channel grids (n = 48, 51.1%) were used followed by 128-channel grids (n = 44, 46.8%). Two 2048-channel grids were used. Grid placement was informed by anatomical landmarks and hypothesis under evaluation with temporal lobe regions being the most common (Table 2). There were 8 instances of PtNRGrid failure across 7 patients where obtained cortical recordings were either unusable or cortical recording could not be performed altogether. Seven such instances were attributed to sterilization related grid damage. One grid was damaged during sterile preparation in the OR after adhering to and ripping surgical gloves. Therefore, 86 of the 94 original grids were used to collect cortical recordings (Table 2).

### Successful Cortical Data Collection and Experimental Testing

Cortical recordings were successfully obtained from 82 patients with 86 functioning grids. Four patients had cortical recordings performed with 2 grids. Grids were most frequently used for recording during experimental research tasks (58.4%) or passive, resting state (Table 1). For those who did have functional testing, most underwent receptive language testing (36.0%) followed by extremity somatosensory and motor testing (27.0%). For patients who underwent research task paradigms most participated in phonemic tasks (33.7%) followed by extremity motor and sensory tasks (23.6%) and passive somatosensory-evoked potential recordings (19.1%) (Table 1).

### V-PRO Sterilization Reduced Instances of PtNRGrid Dysfunction and Maximized Channel Yield

There were 8 instances of grid failure (Table 2). Seven instances involved 1028 channel PtNRGrids and were attributed to grid damage during steam-based sterilization. For context, during the initial few weeks tap water, steam-based autoclaving for PtNRGrids was used. However, inter-institution differences (*investigator personal observations*) in channel yield and impedance, were observed. These may be attributable to locale specific variations in tap water mineral content. This prompted adoption of a V-PRO cycle involving aerosolization of hydrogen peroxide. Improvements in channel performance resulted and no

further encounters or instances of intraoperative grid dysfunction were subsequently noted. Compared to steam-based sterilization, V-PRO conferred significantly superior channel yield (905 [650.8 – 935.5] vs. 356 [18.0 – 597.8], p = 0.0031) for PtNRGrids (Figure 3).

## PEDOT:PSS and PtNRGrids; Not Associated with Intraoperative or Postoperative Adverse Events

There were no instances of intraoperative adverse events or visible tissue damage related to PEDOT:PSS grid or PtNRGrid use. Review of routine postoperative imaging did not reveal any focal abnormalities within or near the cortical regions overlaid by the grids irrespective of grid material composition. Additionally, agnostic of grid material composition, there were no cases of postoperative cranial infections within 90-days after surgery.

## Functional Mapping, Clinical Testing, and Intraoperative Neuro-Monitoring

In this patient cohort, in a patient undergoing awake tumor resection, a 1024-channel PtNRGrid was placed over the central sulcus near the hand region somatosensory evoked potentials (SSEPs) were recorded (Figure 4A). After stimulating peripheral nerves, waveforms with characteristic phase reversal reflective of the M1-S1 functional boundary using both 1024-channel PtNRGrids and 2x8, 16-channel clinical ECoG grids, were captured. Somatosensory evoked potentials (SSEPs) captured on the PtNRGrid had a maximum interpeak amplitude over 20x greater than that of SSEPs capture on a clinical grid and demonstrated a clear phase reversal boundary. The PtNRGrid allowed for visualization of the functional boundary between sensory and motor cortices relative to the canonical anatomical boundary (Figure 4A). Both potential-based and correlation maps provided converging evidence of an offset curvilinear M1-S1 functional boundary indicative of pathological tissue induced functional reorganization.

After phase reversal mapping the M1-S1 boundary, we attempted to map sensory and motor-evoked cortical activity in the same patient. Using an experimental paradigm involving vibrotactile stimulation and a hand grasp task (Figure 4B), the PtNRGrid captured spatiotemporal dynamics of cortical motor and sensory activity with millimeter precision. Vibrotactile stimulation of fingertips elicited a focal increase in high gamma activity (HGA) in the primary somatosensory cortex. There were also spatially distinct patterns of HGA with stimulation of each individual fingertips, allowing us to discern neural correlates of motor activity through hand grasp trials (Figure 4B). Cortical activity captured by the PtNRGrid demonstrated that HGA began in the primary motor cortex before traveling to the M1-S1 functional boundary and ending in the primary somatosensory cortex where it lingered after completion of the grasp motion (Figure 4B).

In another patient with a temporal horn cavernoma undergoing a left temporal lobectomy for intractable epilepsy, PtNRGrid helped identify the seizure onset zone by capturing propagation patterns of seizure activity (Figure 5A). Using vector fields and streamlines, we characterized the spatiotemporal dynamics of spontaneous and bipolar stimulation-induced seizure activity (Figure 5B). We found that vector fields would gain coherence following both spontaneous and stimulation-evoked ictal events. Epileptiform discharges would reliably propagate away from the site of stimulation origin following bipolar stimulation.

Thus, for spontaneous seizure activity, the seizure onset zone could be inferred by tracing the propagated waveforms. For this patient, as indicated on the streamlines plot (Figure 5B), spontaneous seizure activity originated from the right lower corner of the grid, closest to the cavernoma, implicating it as the source of ictal activity. These findings were congruent with the patient's prior stereoencephalography work up, and the epileptogenic tissue was resected as planned.

More recently, we employed a 32 x 32mm 1 mm pitch PtNRGrid and an auditory language testing paradigm to identify neural correlates of auditory language processing during an awake temporoparietal craniotomy for resection of a perirolandic neoplasm (Figure 6A). A PtNRGrid was placed over the patient's left inferior parietal lobe and STG (Figure 6B). Cortical activity captured by the PtNRGrid during auditorily delivered English words was analyzed. We found a robust cortical response to auditory word stimuli 500–600ms following stimuli delivery. When the cortical response captured on the PtNRGrid channels during word stimuli was averaged over this duration, a spatially distinct region of cortical activation could be discerned on the PtNRGrid (Figure 6C). Thus, using the PtNRGrid, we were able to identify a region within the STG that demonstrated preferential engagement in response to auditory language stimuli.

## Discussion

Increasing, improving, and refining ECoG grid resolution capabilities has broad clinical implications of interest to the neurosurgical and neuroscience community, and disease treatment implications for patients. The aim of this study was to demonstrate that use of high-resolution electrode grids can be readily incorporated into a variety of standard of care practice and research settings if pertinent considerations are addressed.

Of the steps involved in the process of microelectrode grid use, we found that the most difficult was establishing a sterilization protocol for PEDOT:PSS grids vs. PtNRGrids. Uguz et al., and Tchoe, Y, et al, note that the optimal sterilization method seems to be dependent on the chemical composition of a given grid.[10,16] As such, we cannot understate the importance of coordinating with hospital sterile processing staff to ensure that sterilization is conducted to optimize electrode performance. To date, no studies have compared the impact of different sterilization modalities on electrode grid parameters such as channel yield and impedance. However, for PtNRGrids in particular, we strongly recommend V-PRO for sterilization. While there is nothing definitively errant *per se* using other sterilization methods, V-PRO has performed the best for PtNRGrids, in our experience, and is readily available at most institutions.

Importantly, throughout our experience, we encountered no instances of adverse events or intraoperative complications related to microelectrode grid use. This was not entirely unexpected given diligent perioperative precautions and grid use that did not require the surgical team to make any substantial modifications, aside from added research time. Subjectively, patients better tolerated the microelectrode grids during passive cortical recording as grids do not need to be pressed down to conform to cortical surface contours.

Notably, there were instances where the PtNRGrids did not function. These instances coincided with the time period immediately prior to implementation of V-PRO sterilization for PtNRGrids and could be attributed to electrode damage incurred during steam-based sterilization. Following the transition to V-PRO, there were no further instances of electrode failure prior to handling. This suggests that PtNRGrids are reliable if sterilized appropriately before use.

The capacity to characterize cortical activity with millimeter precision could have significant implications for surgical management of neurological disorders. Higher resolution ECoG setups may assist with improved demarcation of safe resection zones and mitigate advent of functional deficits following surgeries that either involve or are near eloquent cortical regions.[5,6] This is especially valuable in the context of intracranial neoplastic processes as surgeons work to maximize resection extent to enhance survival without incurring functional deficit(s). Further, intracranial neoplasms, particularly gliomas, are known to induce functional reorganization.[18–20] Tumor induced reorganization may render conventional anatomical landmarks less reliable for functional localization while contemporary mapping tools may have insufficient sensitivity.[21]

Recently, using PtNRGrids Tchoe, Y, et al, better defined the primary somatomotor (M1)-somatosensory (S1) cortical functional boundary, captured sensory and motor spatiotemporal dynamics, and recorded seizure onset and spread with millimeter precision.[10] Locating the functional boundary between motor and sensory cortices, commonly presumed to be central sulcus, is a critical surgical step, especially in the context of tumor resection.

M1-S1 functional boundary localization made possible by the microelectrode grids as described here demonstrates high precision observation and measurements that would have not otherwise been accessible. In this particular example, shift of the functional boundary towards the post-central sulcus indicated the presence of functional motor cortex tissue in the post-central gyrus, which was critically important for the purposes of achieving safe resection. This shift in eloquent tissue was also confirmed with “gold standard”, direct electrical cortical stimulation of this area (*data not presented*). The post-central gyrus is used as a surgical avenue for resection. If in the cases we present, we had assumed eloquent tissue(s) location based on putative gross anatomical demarcations, post-operative functional deficit(s) could have ensued. While current neurosurgical microsurgery is not necessarily performed with millimeter precision, delineating boundaries of safe resection with millimeter resolution opens doors for new, future, high-precision operative techniques.

Obtaining cortical recordings at higher resolutions presents some technical challenges. Contemporary clinical grid systems rely primarily on clinical acumen and human interpretation of captured cortical spectral activity.[22] High resolution grids necessitate use of an automated software-based analysis.[10] Given the high channel count of microelectrode grids, it would be impossible for humans to interpret captured electrophysiologic activity. This represents a potential paradigm shift in real-time intraoperative mapping with a gradual and increasing reliance on higher computational power, which parallels recent trends in bio interface technology advances.[23] This phenomenon of automated analysis of ECoG data is not entirely novel and is available commercially (CortiQ, G tech, Austria),[24] but at a more

modest resolution and requires clinical contextualization. Should high channel count micro electrocorticography be used ultimately for intraoperative functional cortical localization, processing the vast amounts of cortical recording data in near real-time would likely only be possible only through computing capability advancement.[23]

Brain computer interface (BCI) represents another intriguing window of opportunity for microelectrode grid use. BCI configurations that use current clinical ECoG grids are limited by modest spatial resolution.[25] Meanwhile, the microelectrodes described here are capable of capturing brain activity with robust spatial resolution over a physiologically relevant area of the cortex,[10] representing a dramatic improvement upon recordings obtained from previous micro and macro ECoG configurations.[26,27] This allows for better characterization of the spatiotemporal dynamics unique to individual patients and should enhance BCI operation(s). Importantly, whether the PtNRGrids described here are safe for the long-term implantation required of a BCI has yet to be investigated. Further investigation is needed to evaluate the safety profile of microelectrode grids to assess suitability as potential neuroprostheses.

In our experience, we were able to integrate microelectrode grids into surgical workflow seamlessly. However, we stress and emphasize that successful incorporation of microelectrode grids into care is contingent on strong multidisciplinary collaboration between research, clinical, and ancillary staff. Additionally, development of a consistent workflow from order placement to postoperative recovery is imperative.

### Study Limitations

We present data on the first series of patients, to our knowledge, to undergo intraoperative cortical recording with high-resolution microelectrode grids during a craniotomy for pathological tissue resection. The study is limited by the inherent bias of a retrospective design. While this was a multi-institution study, some biases may have affected the results because of patient volume at individual institutions. While, our interpretation of the results are that high-spatial-resolution grids will outperform standard clinical grids with regards to spatial resolution, there were no design experimental comparisons nor were clinical decisions made based upon microelectrode findings. All analyses were *post-hoc*. A guide for grid use is provided, however, we do not provide an overview on how to analyze recorded neurophysiological data. Overviewing spectral analysis techniques is beyond the scope of this article. We refer readers to other comprehensive publications related to this subject.[28] Future investigations will assist with further clarification on the clinical utility of microelectrode grids and better characterize the diagnostic value of high-resolution grids compared to current clinical grids.

## Conclusion

High-spatial-resolution microelectrode grids for cortical mapping can be readily incorporated into neurosurgical craniotomy procedures. Microelectrode grids can potentially provide clinically relevant information about patients and better inform surgical planning. Nonetheless, analyses of postsurgical outcomes following the intraoperative use of these grids will better characterize their clinical value. Special attention to preoperative handling

and sterilization processes helps preserve the number of usable channels and optimizes recording resolution. Further investigations are needed to compare the diagnostic value of these grids to that of clinical grids and extrapolate whether potential diagnostic differences relate to clinical outcomes.

## Supplementary Material

Refer to Web version on PubMed Central for supplementary material.

## Acknowledgments

The authors thank Shirley McCartney, PhD., for editorial assistance.

## References

1. Morshed RA, Young JS, Lee AT, Hervey-Jumper SL. Functional mapping for glioma surgery, Part 2: intraoperative mapping tools. Neurosurgery Clinics. 2021;32(1):75–81. [PubMed: 33223028]
2. Ille S, Krieg SM. Functional mapping for glioma surgery, part 1: Preoperative mapping tools. Neurosurgery Clinics. 2021;32(1):65–74. [PubMed: 33223027]
3. Crone NE, Sinai A, Korzeniewska A. High-frequency gamma oscillations and human brain mapping with electrocorticography. Prog Brain Res 2006;159:275–295. [PubMed: 17071238]
4. Roland JL, Hacker CD, Leuthardt EC. A review of passive brain mapping techniques in neurological surgery. Neurosurgery. 2021;88(1):15–24.
5. Sinai A, Bowers CW, Crainiceanu CM, et al. Electrocorticographic high gamma activity versus electrical cortical stimulation mapping of naming. Brain. 2005;128(7):1556–1570. [PubMed: 15817517]
6. Kojima K, Brown EC, Rothermel R, et al. Clinical significance and developmental changes of auditory-language-related gamma activity. Clin Neurophysiol. 2013;124(5):857–869. [PubMed: 23141882]
7. Maynard EM, Nordhausen CT, Normann RA. The Utah intracortical electrode array: a recording structure for potential brain-computer interfaces. Electroencephalogr Clin Neurophysiol. 1997;102(3):228–239. [PubMed: 9129578]
8. Ganji M, Elthakeb AT, Tanaka A, Gilja V, Halgren E, Dayeh SA. Scaling effects on the electrochemical performance of poly (3, 4-ethylenedioxythiophene (PEDOT), Au, and Pt for electrocorticography recording. Adv Funct Mater 2017;27(42):1703018.
9. Ganji M, Paulk AC, Yang JC, et al. Selective formation of porous Pt nanorods for highly electrochemically efficient neural electrode interfaces. Nano letters. 2019;19(9):6244–6254. [PubMed: 31369283]
10. Tchoe Y, Bourhis AM, Cleary DR, et al. Human brain mapping with multithousand-channel PtNRGrids resolves spatiotemporal dynamics. Sci Transl Med 2022;14(628):eabj1441. [PubMed: 35044788]
11. Yang JC, Paulk AC, Salami P, et al. Microscale dynamics of electrophysiological markers of epilepsy. Clin Neurophysiol 2021;132(11):2916–2931. [PubMed: 34419344]
12. Paulk AC, Yang JC, Cleary DR, et al. Microscale physiological events on the human cortical surface. Cereb Cortex. 2021;31(8):3678–3700. [PubMed: 33749727]
13. Von Elm E, Altman DG, Egger M, et al. The Strengthening the Reporting of Observational Studies in Epidemiology (STROBE) statement: guidelines for reporting observational studies. Ann Intern Med 2007;147(8):573–577. [PubMed: 17938396]
14. Hermiz J, Rogers N, Kaestner E, et al. Sub-millimeter ECoG pitch in human enables higher fidelity cognitive neural state estimation. Neuroimage Aug 1 2018;176:454–464. doi:10.1016/j.neuroimage.2018.04.027 [PubMed: 29678760]

15. Ganji M, Hossain L, Tanaka A, et al. Monolithic and scalable Au nanorod substrates improve PEDOT–Metal adhesion and stability in neural electrodes. Adv Healthc Mater 2018;7(22):1800923.
16. Uguz I, Ganji M, Hama A, et al. Autoclave sterilization of PEDOT: PSS electrophysiology devices. Adv Healthc Mater 2016;5(24):3094–3098. [PubMed: 27885829]
17. Siegle JH, Lopez AC, Patel YA, Abramov K, Ohayon S, Voigts J. Open Ephys: an open-source, plugin-based platform for multichannel electrophysiology. J Neural Eng Aug 2017;14(4):045003. doi:10.1088/1741-2552/aa5eea [PubMed: 28169219]
18. Kristo G, Raemaekers M, Rutten G-J, de Gelder B, Ramsey NF. Inter-hemispheric language functional reorganization in low-grade glioma patients after tumour surgery. Cortex. 2015;64:235–248. [PubMed: 25500538]
19. Charras P, Herbet G, Deverdun J, et al. Functional reorganization of the attentional networks in low-grade glioma patients: a longitudinal study. Cortex 2015;63:27–41. [PubMed: 25241396]
20. Yang J, Kudulaiti N, Chen Z, et al. Within and beyond the visual cortex: brain tumors induce highly sensitive plasticity of visual processing in whole-brain neural functional networks. Cereb Cortex 2022;32(20):4422–4435. doi:10.1093/cercor/bhab492 [PubMed: 35106532]
21. Hong G, Lieber CM. Novel electrode technologies for neural recordings. Nature Reviews Neuroscience 2019;20(6):330–345. doi:10.1038/s41583-019-0140-6 [PubMed: 30833706]
22. Korostenskaja M, Kamada K, Guger C, et al. Electrocorticography-based real-time functional mapping for pediatric epilepsy surgery. J Pediatr Epilepsy 2015;4(04):184–206.
23. Lebedev MA, Nicolelis MA. Brain–machine interfaces: past, present and future. Trends Neurosci 2006;29(9):536–546. [PubMed: 16859758]
24. Prueckl R, Kapeller C, Potes C, et al. cortiQ-Clinical software for electrocorticographic real-time functional mapping of the eloquent cortex. IEEE; 2013:6365–6368.
25. Schalk G, Leuthardt EC. Brain-computer interfaces using electrocorticographic signals. IEEE Rev Biomed Eng 2011;4:140–154. [PubMed: 22273796]
26. Rubino D, Robbins KA, Hatsopoulos NG. Propagating waves mediate information transfer in the motor cortex. Nat Neurosci 2006;9(12):1549–1557. [PubMed: 17115042]
27. Muller L, Piantoni G, Koller D, Cash SS, Halgren E, Sejnowski TJ. Rotating waves during human sleep spindles organize global patterns of activity that repeat precisely through the night. Elife. 2016;5:e17267. [PubMed: 27855061]
28. Mercier MR, Dubarry A-S, Tadel F, et al. Advances in human intracranial electroencephalography research, guidelines and good practices. Neuroimage 2022:119438. [PubMed: 35792291]

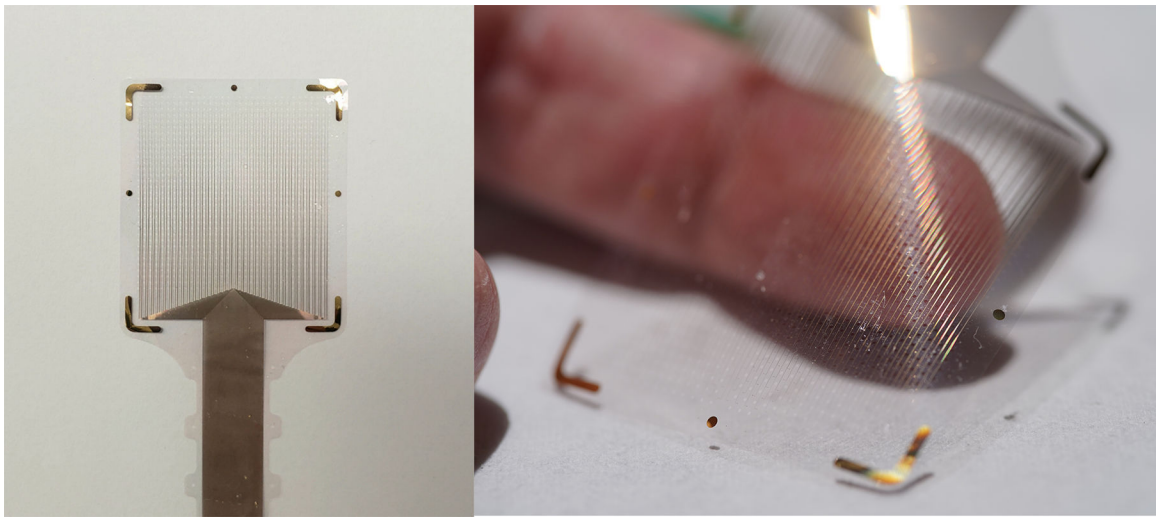

**Figure 1:**
Photos of exemplar microelectrode grids (specifically PtNR grids) used. Note how the electrode contacts are invisible to the naked eye. On the right is a photo of the grid relative to a finger to provide a sense of how compact the microelectrode contacts are.

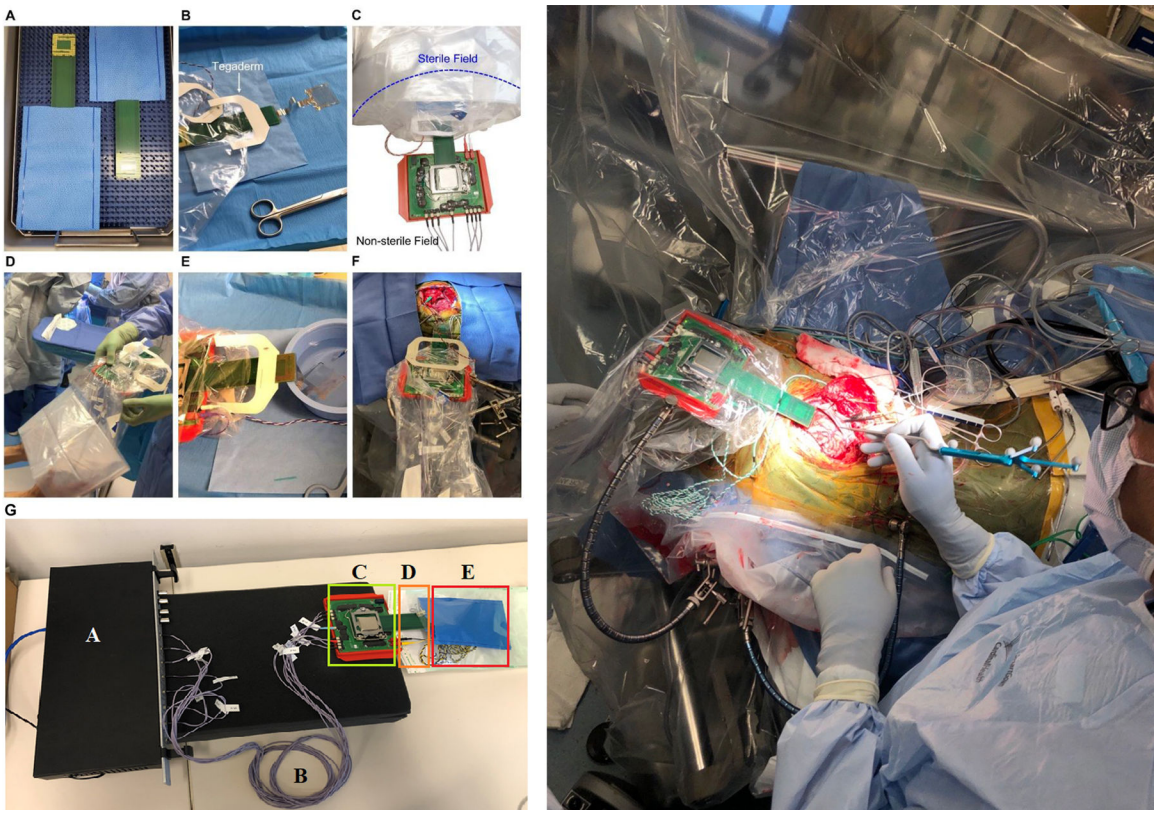


**Figure 2:**

Microelectrode grids in DuraHolder pouches placed in a sterilization tray (A). The extension board passed through the Situate™ Sterile Drape and secured by Tegaderm to create a sterile barrier (B). The green extension board is then connected to an amplifier board (C) and the drape is then pulled from the inner, nonsterile surface by a team member such that it covers the amplifier board and associated outgoing cables (D). Impedance and channel yield testing is then performed with sterile saline (E). Once properly positioned, Greenberg or C clamps are used to secure the amplifier board in place (F). The recording set-up is depicted in (G). The Intan amplifier, **A**, is connected to the amplifier board via 8 SPI cables, **B**. The amplifier board, **C**, is connected to the extension board and grid, **D** and **E** respectively. The right panel showcases the usage of microelectrode grids intraoperatively by the senior author. Adapted with permission from Tchoe et al. 2022.[7]

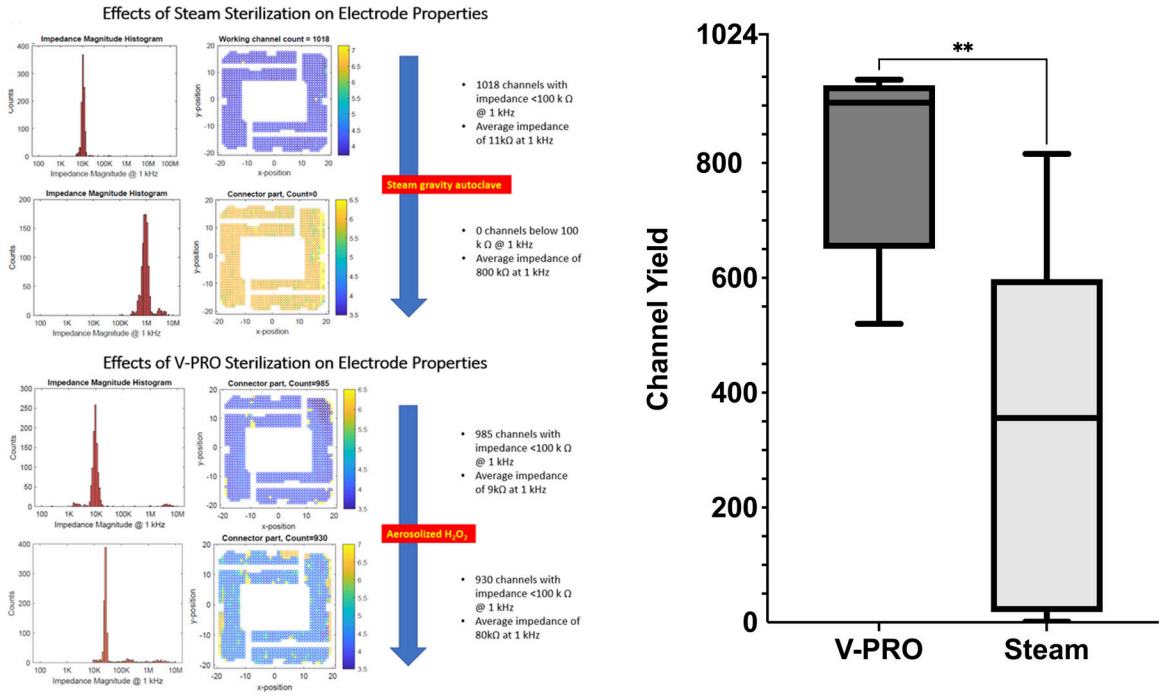


**Figure 3:**

Influence of sterilization modalities on PtNR grid impedance and channel yield Left panel presents exemplar outputs from an in-house MATLAB script used to conduct impedance and channel yield testing on PtNR grids. Note the greater median impedance magnitude increase (see in-laid Impedance Magnitude Histograms) following steam autoclaving compared to V-PRO. Right panel shows the difference in usable channels following V-PRO and steam-based sterilization methods. Non-parametric Mann-Whitney U-test comparing channel yield of PtNR grids sterilized via steam (n = 7) vs. V-PRO (n = 20) indicated that V-PRO preserved significantly more channels (905 [650.8 – 935.5] vs. 356 [18.0 – 597.8], p=0.0031).

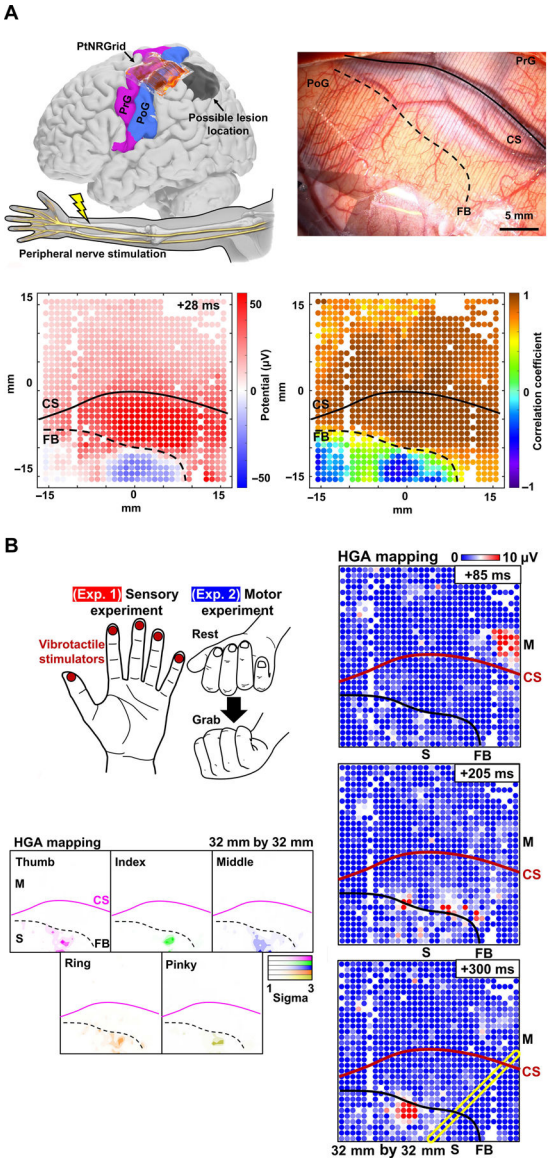


**Figure 4:**

PtNR microelectrode grid placement with the discrepancy in central sulcus vs. phase reversal identified M1-S1 functional boundary displayed (A). Top right left and right panels show grid placement and the position of the identified functional boundary (FB) relative to the central sulcus (CS), respectively. Bottom panels show FB vs. CS relationship identified through potential-based, left, and correlation coefficient maps, right. Schematic of sensory and motor experimental paradigm with associated findings (B). Bottom left quintet of panels show the localization and intensity of HGA for each fingertip in response to vibrotactile stimulation. The right vertical three panes show the progression of HGA over the primary motor and sensory cortical regions at 85ms, 205ms, and 300ms following hand grasp initiation. Adapted with permission from Tchoe et al. 2022.[7]

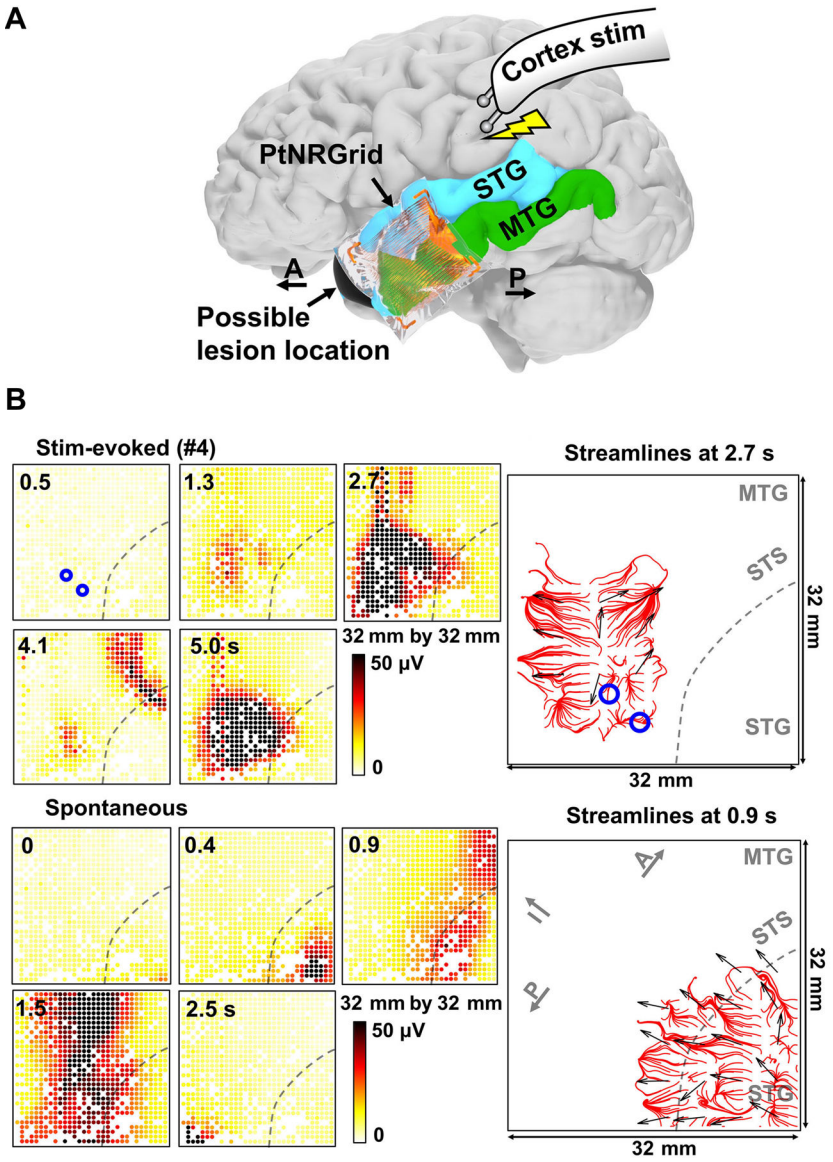


**Figure 5:**

PtNR microelectrode grid placement relative to the potential seizure focus, superior temporal gyrus (STG) and middle temporal gyrus (MTG) (A). Stimulation-induced and spontaneous ictal cortical discharges captured on microelectrode grid (B). Left panels show temporal changes in stimulation and spontaneous evoked brain wave amplitudes while streamlines plots are presented on the right with arrows indicating the direction of brainwave spread. Adapted with permission from Tchoe et al. 2022.[7]

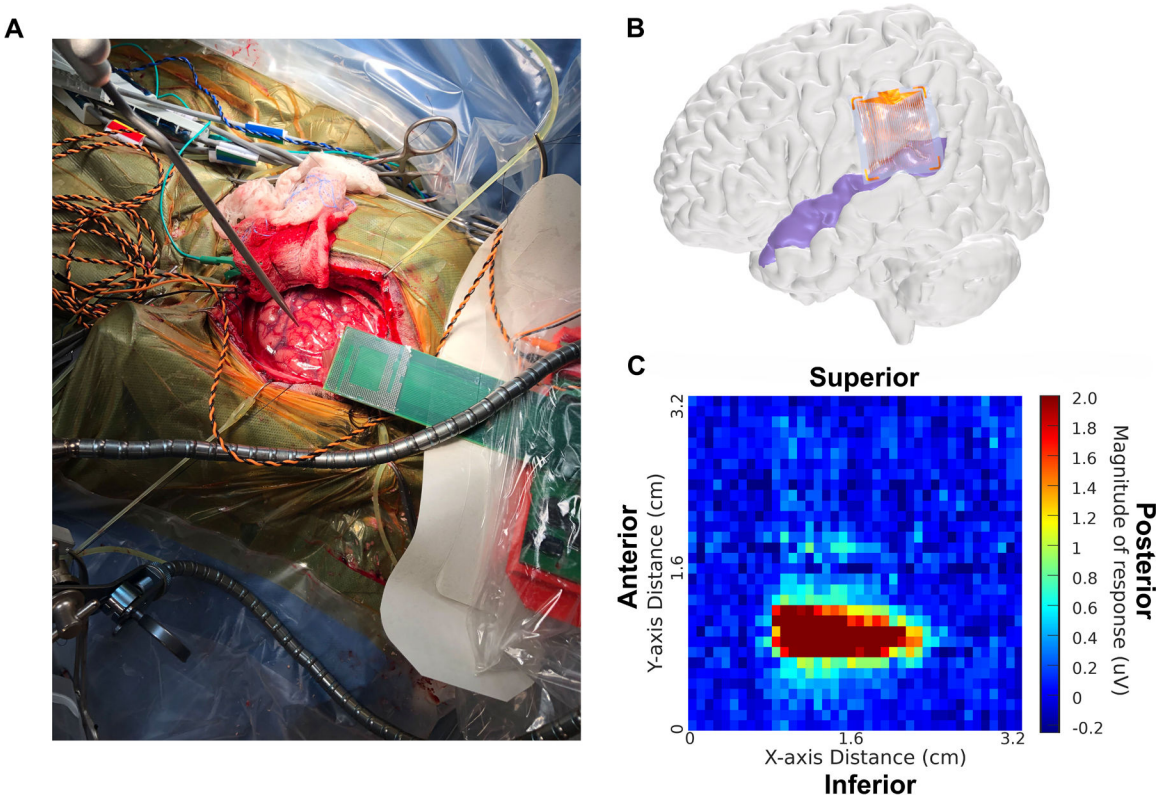


**Figure 6:**

Intraoperative photograph showing the placement of the PtNR microelectrode grid in relation to the temporoparietal craniotomy (A). Illustration depicting the placement of the PtNRGrid in relation to the superior tempooral gyrus (STG) which is colored light purple (B). Heat map showing the degree of mean cortical response 500–600ms after auditory language stimuli delivery across PtNRGrid channels (C). Note the horizontal oblong region of particularly strong response shown in dark red.

**Table 1:**

Patient demographic, clinical, operative and intraoperative testing data.

| Variable | Data value | Distribution and frequency¶; total n = 89 patients, n (%) |
|---|---|---|
| **Age (years)** | | 45.9 ± 1.7 |
| **Sex** | | |
| | Male | 47 (52.9) |
| | Female | 42 (47.1) |
| **Institutional site** | | |
| | OHSU | 56 (63.0) |
| | MGH | 22 (24.7) |
| | BWH | 8 (8.9) |
| | UCSD | 3 (3.4) |
| **Surgical indication** | | |
| | Intracranial neoplasm | 58 (65.2) |
| | Intractable epilepsy | 31 (36.8) |
| **Pre-operative deficits** | | |
| | None | 62 (69.7) |
| | Motor | 21 (23.6) |
| | Visual field | 7 (7.9) |
| | Sensory | 5 (5.6) |
| | Language | 4 (4.5) |
| | Cognitive | 3 (3.4) |
| **Anesthesia** | | |
| | Monitored anesthesia care | 61 (68.5) |
| | General anesthesia | 28 (31.5) |
| **Clinical mapping** | | |
| | Phase reversal | 45 (50.6) |
| | Passive high gamma | 50 (56.2) |
| | Electrical stimulation | 52 (58.4) |
| | Subcortical | 11 (12.4) |
| **Intracranial recording setting** * | | |
| | Evoked response | 11 (12.4) |
| | Experimental task | 52 (58.4) |
| | Resting state | 32 (38.1) |
| **Functional domains tested** | | |
| | Receptive language | 32 (36.0) |
| | Facial sensorimotor | 5 (5.6) |
| | Extremity sensorimotor | 24 (27.0) |
| | Visual | 1 (1.1) |
| | Not assessed | 32 (36.0) |
| **Research tasks** | | |
| | Phonemic | 30 (33.7) |

| Variable | Data value | Distribution and frequency¶; total n = 89 patients, n (%) |
|---|---|---|
| | Extremity motor/sensory | 21(23.6) |
| | Facial motor/sensory | 2 (2.2) |
| | SSEP recording | 17(19.1) |
| | Stimulation via electrode grid | 8 (9.0) |
| | Other/improvised | 7 (7.9) |
| | None | 31 (34.8) |

Frequencies are presented as mean ± standard error or count (% of all patients) when applicable. Note that for categorical variables where tallies for multiple categories can apply for a given patient, a (%) is not given.

**Abbreviations**: Oregon Health & Science University (OHSU), Massachusetts General Hospital (MGH), Brigham Women's Hospital (BWH), University of California San Diego (UCSD), Somatosensory Evoked Potential (SSEP)

*encompasses fence post technique (n = 1) and subcortical stimulation (n = 1)

**Table 2:**

High-resolution microelectrode grid characteristics and use.

| Characteristics | Level | Distribution and frequency[¶]; total n = 94 grids, n (%) |
|---|---|---|
| **Intraoperative grid use** | | |
| | Success | 86 (91.5) |
| | Failure (PtNRGrid) | 8 (8.5) |
| **Channel count & grid dimensions** | | |
| | 128-channel[+] | 44 (46.8) |
| | - 2x64 contact columns (50 μm pitch) | 32 |
| | - 2x64 contact columns (800 μm pitch) | 1 |
| | - Circular, 4mm diameter | 11 |
| | 1024-channel (32mm x 32mm) | 48 (51.1) |
| | 2048-channel (48mm x 48mm) | 2 (2.1) |
| **Chemical composition** | | |
| | PEDOT:PSS (Patients, n = 57) | 58 (61.7) |
| | PtNRGrid (Patients, n = 25) | 36 (38.3) |
| **Grid placement**[*] | | |
| | Rolandic | 10 (10.6) |
| | Temporal lobe[++] | 39 (41.5) |
| | - Posterior STG | 12 (12.8) |
| | - Anterior STG | 2 (2.1) |
| | Temporoparietal | 8 (8.5) |
| | Extra-Rolandic parietal | 4 (4.3) |
| | Prefrontal lobe | 10 (10.6) |
| | Occipital | 2 (2.1) |
| | Overlying pathology | 2 (2.1) |
| | Multiple locations (relocated) | 13 (13.8) |
| **Placement strategy**[*] | | |
| | Anatomical landmarks | 67 (71.3) |
| | Passive gamma mapping | 18 (19.1) |
| | Direct cortical stimulation | 3 (3.2) |
| **Recording duration (minutes)** | | 15.3 ± 1.15 |

[¶]Frequency presented as mean ± standard error or count (% of all grids)

[*]The 8 PtNRGrid failures are not tallied and reported under these categories.

[+]Includes the 50μm and 800μm 2x64 contact column as well as the circular 128-channel grids

[++]Includes posterior and anterior STG counts

**Abbreviations:** Poly(3,4-ethylenedioxythiophene) with polystyrene sulfonate (PEDOT:PSS), Platinum Nano-rod (PtNRGrid), Superior temporal gyrus (STG), primary motor cortex (M1), primary sensory cortex (S1)